

A Mini Review of the Key Components used for the Development of High-Speed Atomic Force Microscopy

Wei Cai, Zhengliang Liu, Yan Chen, and Guangyi Shang*

*Department of Applied Physics, Beihang University, Beijing 100191, People's Republic of China;
Key Laboratory of Micro-Nano Measurement-Manipulation and Physics (Ministry of Education),
Beihang University, Beijing 100191, People's Republic of China*

ABSTRACT

Dynamic phenomena on nanoscale have continuously attracted attention from various research fields. However, due to the limit of the imaging rate, it is difficult to observe the dynamic processes by conventional atomic force microscope (AFM). In recent years, a considerable variety of important improvements on the AFM system for high-speed imaging have been proposed and demonstrated. In this mini review, we briefly present the latest research works on the development of high-speed AFM (HSAFM) from the view of instrumentation. Besides commercially available instruments, many schemes for the design and construction of HSAFM system for different applications are summarized. Also, the low-cost hardware and software upgrading options from conventional AFM to HSAFM are compared. Furthermore, the requirements for each component in the AFM control loop are analyzed. Finally, challenges and future works of HSAFM are discussed. This review would be beneficial for the development of new HSAFM imaging systems.

KEYWORDS: Atomic Force Microscopy, High-Speed Atomic Force Microscopy, Scanning Probe Microscopy, Surface Analysis.

CONTENTS

1. Introduction	77
2. Components for high-speed AFM	79
2.1. High Frequency Small Cantilevers	79
2.2. Improvement of the Optical Beam Deflection	80
2.3. XY Scanner	81
2.4. Z-Scanner	83
2.5. Electronic System	85
3. Conclusion and Outlook	86
Acknowledgments	86
References and Notes	86

1. INTRODUCTION

As a branch in the family of scanning probe microscopy (SPM), atomic force microscopy (AFM), which uses a very sharp tip at the end of a cantilever to probe the properties of the sample surface at the micro- and nanoscale under various conditions, has been widely used in a lot of research fields. Since it was invented in 1986 by Binnig, Quate, and Gerber,¹ modern AFM has been equipped with various kinds of probes and measurement modes.

Different properties of the sample surface, e.g., mechanical, electrical, and magnetic information, can be detected and characterized nowadays.² However, the imaging speed of AFM still seriously limits its applications. Usually at least several minutes are needed to acquire an acceptable image for most users.³ With traditional AFM, it is difficult to observe the dynamic events happened on the sample surface, such as the crystallization processes of the polymer materials, the changes in the structure and dynamics of biological molecules.^{4–6} In addition, for large-area surface survey or inspections used in industry and AFM probe-based nano-fabrications, the imaging speed is also a bottleneck.⁷

AFM is a mechanical microscope.⁸ With the help of a nano positioning unit which usually consists of piezo elements, the tip or the sample can be moved relatively in three dimensions with nanometer resolution. The interactions between the tip and the sample are collected and processed point by point and thus images describing the surface properties are constructed. The major factors that limit the imaging speed of AFM involve the measurement bandwidth of the local interactions between the tip and sample (the resonance frequency or bandwidth of the probe), the rate at which the tip can scan the sample surface in the *xy* plane (the resonance frequency or bandwidth of

* Author to whom correspondence should be addressed.
Email: gyshang@buaa.edu.cn
Received: 26 December 2015
Accepted: 17 March 2016

the scanner), and how quickly the tip can follow the contours of the sample surface (the closed-loop bandwidth of vertical feedback).⁸ The final imaging speed is determined by the slowest component in AFM's entire control loop.³ By making the improvements of each factor that limits the imaging speed, Ando et al. reported the first HSAFM (High-speed AFM) system that could image at more than 1000 lines per second.^{7,9} Over the last decade, a considerable variety of important improvements have been proposed and demonstrated. The techniques and instrumentation to increase the AFM imaging speed, historical overviews of HSAFM's development stages, and the

dynamic behaviors observation in material science and biological applications are reviewed in several recent publications.^{10–12}

Although the commercial implementations are becoming available now, it would be necessary to develop a home-made HSAFM system for special use in one's own laboratory. In this mini review, we aim to describe and explain the components and key techniques for the development of HSAFM from the view of instrumentation. We hope that this mini review would be helpful for researchers from various fields who are interested in HSAFM and its applications.



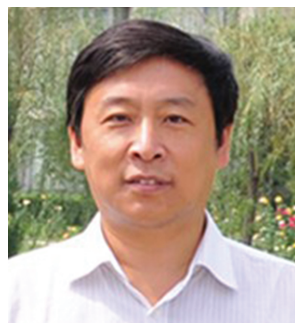
Wei Cai received his Ph.D. degree in School of Physics from Beihang University under the supervision of Professor Junen Yao and Professor Guangyi Shang in 2011. Currently he is a Lecturer at the Department of Applied Physics in Beihang University. His research interests focus on micro-nano measurement and materials characterization by scanning probe microscopy.



Zhengliang Liu received his bachelor degree in school of Mechatronic Engineering and Automation from Shanghai University in 2011. Now he is a Ph.D. student at the Department of Applied Physics of Beihang University under the supervision of Professor Guangyi Shang. His main research interests are electrochemical atomic force microscopy and its control methods.



Yan Chen received his master degree in School of Physics from Beihang University in 2006. He is currently a Lecturer in the Physics Experiment Center of Beihang University. His major research interests are electronics system and automation.



Guangyi Shang is a Professor at the Department of Applied Physics, Beihang University. Professor Shang's research focuses on advanced characterization method by scanning probe microscopy and its applications in materials science and condensed matter physics at nanoscale.

Table I. Comparison between HSAFM and conventional AFM.

	Conventional AFM	HSAFM
Cantilever type	Standard cantilever	Small cantilever
Cantilever resonance	~5–300 kHz	~0.7–6 MHz
Laser focal spot size	~50 μm	~10 μm or smaller
Line scan rate	~0.1 Hz–several Hz	~0.1 kHz–several kHz
Actuator type	Piezo tube	Piezo stacks
Scanner resonance	~5 kHz	~30–600 kHz
Feedback bandwidth	~100 Hz	~100 kHz
Data acquisition rate	~500 kHz	~1.3–3.3 MHz

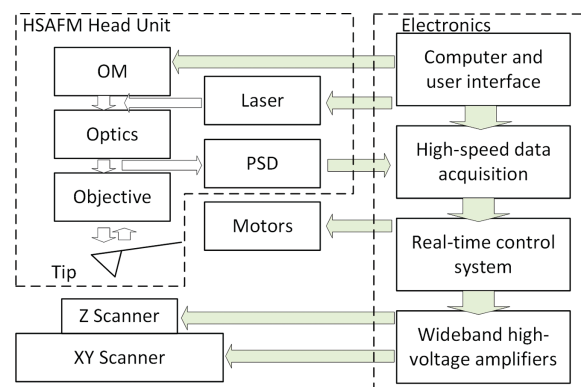
For comparison, we list some differences between conventional AFM and HSAFM. As shown in Table I, there are many parameters which indicate the improvement of AFM, e.g., the cantilever resonance frequency, the scan rate, and the bandwidth of control system. The reason for this is the probe, the scanner, and the electronics of HSAFM are redesigned to reduce their response time in imaging. So this paper is organized as follows. In Section 2 we mainly focus on the components for the construction of HSAFM. In Section 2.1 we discuss the high-frequency small cantilevers. In Section 2.2 we analyze the improvements of the optical beam deflection in HSAFM. In Section 2.3 we describe the *XY* scanner including the flexure-guided scanner and the resonance-type scanner. In Section 2.4 we describe the *Z*-scanner design in HSAFM. In Section 2.5 we introduce the electronic system including the wideband high-voltage amplifier, the high-speed data acquisition system, and the feedback controller. Finally, the conclusion and the outlook are given in Section 3.

2. COMPONENTS FOR HIGH-SPEED AFM

The dynamics of components in the feedback control loop which include the cantilever, the scanner, the piezo drivers, the feedback controller, and other electronics, would limit the imaging speed of AFM.¹¹ Briefly speaking, the response of electrical parts is usually faster than mechanical ones. So the main bottlenecks that limit the imaging speed are the cantilever and the scanner.¹³ To increase the imaging speed, the resonance frequencies of the cantilevers and scanners need to be improved. If the structure and the response time of the mechanical parts are updated, the corresponding electronics system should also be compatible with the improvements, including the wideband high-voltage amplifiers, high-speed data acquisition and control system. The schematic drawing of HSAFM system is shown in Figure 1.

2.1. High Frequency Small Cantilevers

The dynamics of the AFM cantilevers can be briefly described by Euler–Bernoulli beam theory.¹⁴ The resonance frequency and spring constant of the cantilever can be evaluated by using Eqs. (1) and (2). The method to increase the

**Fig. 1.** Schematic drawing of HSAFM system. OM and PSD are optical microscope and position sensitive detector, respectively.

resonance frequency f_c , from Eq. (1) is to reduce the length L of the cantilever, which can effectively increase the resonance frequency f_c . However, from Eq. (2), if keeping other dimension parameters like the width w and the thickness d of the cantilever constant, the spring constant k_c would be increased too, which is undesirable because the harder cantilever would increase the interaction forces between the tip and the sample during imaging. For some fragile samples like biological cells and membranes, larger interaction force during scanning might damage the sample surface. The optimal method is to reduce all the geometric parameters of the cantilever to improve its resonance frequency f_c while still keep the spring constant k_c small enough.

$$f_c = 0.56 \frac{d}{L^2} \sqrt{\frac{E}{12\rho}} \quad (1)$$

$$k_c = \frac{wd^3}{4L^3} E \quad (2)$$

The early research work on fabricating small AFM cantilevers carried out by Hansma's group and Ando's group can be found in Refs. [7, 12, 15]. Table II summarizes several commercially available small AFM cantilevers which have been used in recently published literatures. For example, Liao et al. used the NanoWorld's (Switzerland) "ultra-short" cantilevers in their home-made high-speed AFM. The dimension of the cantilever is $10 \times 5 \times 0.68 \mu\text{m}$. The

Table II. Typical commercially available small cantilevers and their specifications.

Model	$L \times w \times d$ (μm)	f_c (MHz)	k_c (N/m)	References
USC-F5-k30, NanoWorld	$10 \times 5 \times 0.68$	5 (4–6)	30	[13]
BL-AC10DS-A2, Olympus	$9 \times 2 \times 0.13$	1.5	0.1	[11, 18]
FASTSCAN-A, Bruker	$27 \times 33 \times 0.58$	1.4 (0.8–2.0)	18	[17, 20]
ARROW-UHF, NanoWorld	$35 \times 42 \times 0.7$	1.5 (0.7–2.0)	/	[16, 19]

measured resonance frequency is ~ 5.5 MHz in air.¹³ Cantilevers with the resonance frequency of ~ 1.5 MHz can be obtained from several manufacturers.^{11,16–20} As shown in Table II, “BioLever fast” from Olympus (Japan), which can be used for dynamic biological processes such as living cell imaging,^{11,18} has the smallest spring constant of ~ 0.1 N/m. “Fastscan-A” provided by Bruker has a trapezoidal plate geometry with the dimension of $27 \times 33 \times 0.58$ μm . The nominal resonance frequency is ~ 1.4 MHz and the spring constant is 18 N/m.^{17,20} Previous research supported that the trapezoidal-plate geometry is ideal for high-speed applications, resulting in cantilevers with high resonance frequency, high Q factor, low spring constant, and a large region for the laser spot.^{21,22} An overview of the commercially available small cantilevers is provided in the supplementary material of Ref. [23]. Custom-made cantilevers with high frequency and small spring constant can also be found. For example, a high-end small cantilever (BL-AC7DS-KU2, custom-made, Olympus) has been routinely used for imaging studies in Ando’s group. The cantilever has the size of $6\text{--}7 \times 2 \times 0.09$ μm , the resonance frequency of 3.5 MHz in air and a spring constant of 0.2 N/m.^{18,24}

The response of the cantilever is not the slowest in AFM control loop, so very soft and flexible contact-mode cantilevers can also be used in some specific systems (using contact mode deflection measurements) despite their relatively low resonance frequency (~ 10 kHz). For example, Miles’s group selected a contact mode cantilever (MSNL, cantilever C, Bruker) for imaging. The first resonance frequency of the 310 μm long triangle cantilever is ~ 7 kHz and the spring constant of that is 0.01 N/m.^{25–28} Seo et al. used a Si_3N_4 cantilever (Biolever, Olympus) which has a resonance frequency of ~ 13 kHz and a spring constant of 0.006 N/m.^{29,30} In the experiments of our group, a small rectangular cantilever (BL-AC40TS-C2 Biolever-mini, Olympus) was used, whose resonance frequency in air and spring constant are typically 110 kHz and 0.1 N/m respectively.^{31–36} The cantilevers with larger spring constant were employed for imaging hard samples, such as NT-MDT NSG03 cantilever (90 kHz, 0.5 N/m)³⁷ and Olympus Biolever TR800PSA (73 kHz, 0.57 N/m).³⁸ Tap190Al-G with the first resonance frequency of 190 kHz and force constant of 48 N/m was also used to image grating samples.^{38,39}

2.2. Improvement of the Optical Beam Deflection

Because the size of the cantilever has been reduced to be smaller than that of the usually used laser spot, the optical beam deflection (OBD) method needs to be improved correspondingly. The aim of the improvement is to focus the laser beam on the cantilever with the spot size of ~ 10 μm . For Gaussian beams, the focused spot size can be evaluated by the width of the beam waist w_0 which is

related to the numerical aperture N.A. of the objective lens (Eq. (3)). So the lens with a high N.A. is required to effectively reduce the size of the laser spot. Table III shows the summary of the types of the focusing lens used in HSAFM optical beam deflection systems.

$$w_0 \approx \lambda / (\pi \text{N.A.}) \quad (3)$$

In the early work of Hansma’s group,^{40–42} a collimated laser was focused on the cantilever by three lenses. One of the lenses is movable for focus adjustment. The lens placed close to the cantilever has a large N.A. and its working distance is very small (several millimeters), so the incident and reflected light would pass the same lens. With the help of polarization beam splitter and $\lambda/4$ wave plate, the incident light and the reflected light can be separated and the spot size can be further reduced because of polarization.⁴² This scheme has been widely adopted in the following designs.^{7,12,43} For example, Adams et al. used two aspheric lenses (N.A.=0.53, working distance is 4.6 mm), one polarizing beam splitter, and one $\lambda/4$ wave plate to develop a polarization-based separated light path. The $1/e^2$ waist measured by the knife-edge method is ~ 1.9 μm .²⁰ The schematic of the light path is shown in Figure 2(a).

$$\text{DOF} = w_0 / \text{N.A.} \quad (4)$$

Small laser spot results in small depth of focus (DOF, see Eq. (4)), so one has to refocus the laser spot on the back of the cantilever after changing the probe. High quality viewing system would be helpful if it is arranged confocal with the incident beam. If one adjusts the focusing lens in such way that the cantilever appears in focus, then the incident beam is focused on the plane of the cantilever as well.⁴²

In the scheme of Ando’s group, a commercial objective has been used to focus the laser beam onto the small cantilever. For example, the OBD is combined with the optical path of an inverted optical microscope.^{7,11} In these configurations, the AFM’s structure is inverted too. Commonly, the cantilever has a small tilt angle of $\sim 10^\circ$ relative to the horizontal plane to make sure the tip-end contacts the sample surface first. So in order to collect the reflected light

Table III. The focusing lens used in the optical beam deflection of HSAFM.

	Type	N.A.	WD (mm)	Diameter (mm)	References
ELWD 20XC, Nikon	Objective	0.45	8	\	[10]
L Plan 20X SLWD, Nikon	Objective	0.35	24	\	[11, 44, 45, 48]
A390-A, Thorlabs	Aspheric lens	0.53	4.6	6	[20]
Convex lens	Convex lens	0.4	~ 5	4.5	[52]

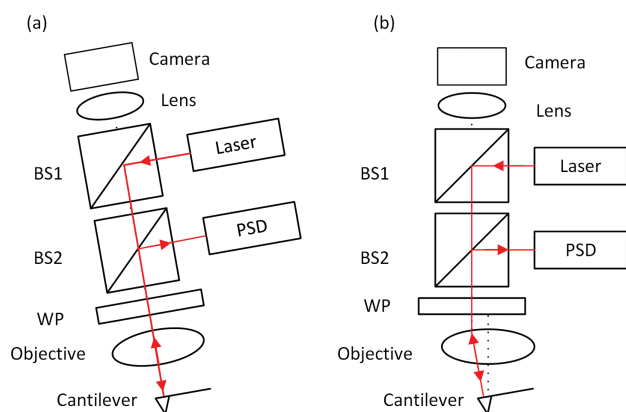


Fig. 2. Schematics of the polarization-based optical beam deflection methods. (a) On-axis and (b) off-axis light paths are shown, respectively. The optical component BS means beam splitter and WP means quarter-wave plate.

with the same objective, the incident beam on the objective lens has an off-centered position.⁷ Then the outgoing beam can be focused on the back of cantilever vertically and the reflected light can go back with the same light-path. Off-centered incident beam with upright optical microscopes can also be found in recent publications.⁴⁴ The schematic of the light path is shown in Figure 2(b). Alternatively, the sample placed over the cantilever has a tilt angle of $\sim 10^\circ$ relative to the horizontal plane⁴⁵ while the cantilever can be placed parallel to the horizontal plane. And in the design with long-working-distance objective, the reflected light does not have to pass through the same lens and the PSD (position-sensitive detector) can be set up on one side of the objective.^{46, 47}

Sample-scan AFM has several restrictions on the expansion of its applications. For example, the sample size is limited. The sample mass would reduce the imaging rate, and the moving sample makes simultaneous HSAFM/fluorescence-microscopy observation impossible.⁴⁸ Therefore, the tip-scan mode of HSAFM has been developed and the key technique in tip-scan optical path is the laser beam tracking method.^{49–51} One popular solution is the use of a small focusing lens embedded in the XY-scanner.⁵² In the commercially available instrument, similar design can also be found.¹⁷ Another sophisticated method is using a tilting reflection mirror to track the lateral motion of the cantilever.^{48, 53} The tilt angles of the mirror placed in optical path between the cantilever and the photodiode sensor can be changed in synchrony with XY scanning of the cantilever.⁴⁸ Furthermore, in some tip-scan HSAFM configuration, laser tracking is not used because noticeable misalignment of the laser beam path has not been found when the scan range is limited within the size of the laser spot.^{29, 32–34}

2.3. XY Scanner

Four-segmented piezoelectric tube scanner is the most widely used nano-positioner in scanning probe microscopy.⁵⁴

It has a compact structure and provides three dimensional movements with only one piezo-component. However, since the tube scanner has a very low lateral resonance frequency (< 1 kHz), the scan speed is limited to several Hz with triangle driving waveforms. If the scan speed increases, mechanical vibrations take place, which will result in serious distortion of the scanned images.⁵⁴ Shear piezo can be used as high-speed lateral scanner and its structure is compact too. However, the scan size is very small ($< 1 \mu\text{m}$) for practical application.⁵⁵ In order to develop faster scanners suitable for HSAFM, two types of scan hardware have been proposed and demonstrated. One is the piezo stacks driven and flexure-guided scanner. The other is the resonance-type scanner. The advantages and disadvantages of these scan hardware can be found in recent reviews.^{10, 11, 56} Here, we summarize these two types of methods as below.

2.3.1. Flexure-Guided Scanner

Flexure-guided nano-positioners meet the demand for high-speed and high-accuracy nanoscale positioning. The development of high-bandwidth and flexure-guided nano positioning systems can be found in recently published review paper.⁵⁷ The key techniques in flexure-guided scanners involve the “blade spring” or “comb-flexures” structures and the piezo stack actuators. Based on the differences in structure, flexure-guided scanner can be categorized into two main configurations: serial and parallel.⁵⁷

In the scheme of Ando’s group, serial-kinematic configuration was used. The X, Y, and Z-piezo stacks have different resonance frequencies and scan ranges. In the design of the ball-guide stage, the Y-piezo displaces base-1 on which the X- and Z-scanners are mounted, while the X-piezo displaces base-2 on which the Z-scanner is mounted.⁷ This design has been enhanced with flexure (blade springs) structures which are not only sufficiently flexible to be displaced but also rigid in directions perpendicular to the displacement axis. The Y-piezo (slow axis) pushes the XZ-block that is connected to the base frame with two pairs of flexures. While within the XZ-block, the X piezo (fast axis) displaces the block of Z-scanner which is also connected to the frame of the XZ-block with a pair of flexures.^{10, 11, 53} The schematic of the serial structure is shown in Figure 3(a). This asymmetric structure has some advantages like it does not suffer from parasitic, off-axis motion and can minimize crosstalk between the three-axis displacements.⁵³

In the design of Hansma’s group, parallel-kinematic configuration was employed. The schematic is shown in Figure 3(b). The “comb-flexures” scanner has symmetric structure where the center of the mass was in the axis of the whole structure. This would provide extra mechanical and thermal stability.⁵⁸ Another advantage is the fast axis of a parallel nanopositioner can be chosen arbitrarily in experiments. Additionally, parallel-kinematic systems can also be used for emerging non-raster scan methods.^{57, 59–62}

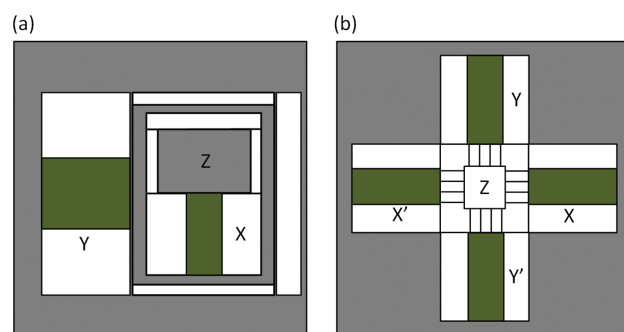


Fig. 3. Schematic of the flexure-guided and piezo-stacks driven scanners. (a) and (b) are serial and parallel structure, respectively.

However, this configuration is usually apt to suffer from crosstalk between X - and Y -axis.⁵⁷ One solution is to decouple the motion between the X and Y piezos with ball bearings.⁶³ Similar design with longer piezo stack actuators for larger scan range^{16,28} and the devices equipped with capacitive position sensors were also reported.^{64–68} In Miles's group, custom-designed XY scan stage driven by piezo stacks within a 2D flexure guidance system was also proposed recently.⁶⁹

For wider-area scanning ($>20 \times 20 \mu\text{m}^2$), mechanical amplification devices are needed because the displacement range of piezo stack actuators with dimensions adequate for HSAFM systems is limited.^{24,70} The mechanical amplifiers in XY scanner might lower the mechanical resonance frequencies and thus lower the scanner's bandwidth. To achieve a high resonance frequency, the design of nano positioner has to be compact and rigid.⁵⁷ The geometry parameters would also limit the scanner's resonance frequency, e.g., shorter flexures can get higher resonance frequency hence higher bandwidth. But shorter flexures will reduce the scan range of the piezo stacks. In flexure scanner's design, FEA (finite element analysis) simulation would be helpful to determine the resonance frequency of the assembly of flexure structures and piezo stacks. Also with the help of FEA simulation, the structure and the geometries can be optimized.^{16,66,67,71,72}

Considering from the view of data-collection system,⁷³ provided that the target is to obtain an image with $N \times N$ pixels resolution and the imaging speed is evaluated by FPS (frame per second), then the line scan rate f_x (frequency in fast axis) and the frequency in slow axis f_y can be calculated by the following equations:

$$f_x = N \times \text{FPS} \quad (5)$$

$$f_y = \text{FPS} / 2 \quad (6)$$

The unit is Hz. For example, if the pixel resolution is 256×256 and the target imaging speed is 25 FPS, the desired frequency of fast axis is 6400 Hz (6.4 kHz) and that of slow axis is 12.5 Hz.⁷³ In practical designs, the resonance

frequency of fast axis of the scanner is three times larger, which is up to ~ 20 kHz. So the components of the piezo stacks for XY scanner which should have the unload resonance frequencies of more than ~ 100 kHz, are usually selected. For example, AE0505D08 from NEC-tokin (or Thorlabs) has the unload resonance frequency of ~ 138 kHz with the maximum displacement of $\sim 9 \mu\text{m}$.^{48,53,74} Similarly, piezo stacks from Piezomechanik (PSt 150/5 \times 5/7 and PSt 150/7 \times 7/7), which have the unload resonance frequency of ~ 100 kHz with the maximum displacement of $\sim 13 \mu\text{m}$, were employed.^{13,16} And the piezoelectric stack actuators from Noliac (SCMA-P7, 5 \times 5 \times 10 mm, 380 nF) with unload resonance frequency larger than ~ 250 kHz were used to increase stiffness of the scanner.⁷⁵

2.3.2. Resonance-Type Scanner

Instead of building rigid XY scanners, the other type of the fast scanner is the resonance-type scanner. It can be fabricated by using a small mechanical oscillator as the fast scan axis, such as a tuning fork firstly proposed by Humphris et al. in Miles's group,^{8,76,77} a brass bar,²⁹ a quartz bar,⁷⁸ or a bimorph beam.^{31,32} These scanners provide fast scan motion at their resonance frequencies rather than getting far away from them,¹² and serve as fast axis of the XY scanner. Another piezo actuator or one axis of the tube scanner can be served as slow scan axis. Usually, the sample size is limited within the scope which is comparable to that of the oscillator. Also lightweight samples are often required. Otherwise, the mechanical properties of the fast scanner would be changed a lot after the sample was attached to it. Tip-scan configuration combined with the resonance-type scanner can be used to solve this problem.^{29,32} Schematics of sample-scan and tip-scan configurations based on the resonance-type scanners are shown in Figures 4(a and b), respectively. The notable advantages of the resonance-type scanners include:

- (i) a simple structure of the scanner which is easy to be fabricated, like bar-shape and beam-shape;
- (ii) a large scan range; and
- (iii) a low drive voltage with sinusoidal waveform, where high-voltage wideband amplifiers are not necessary for fast scan axis.³⁵ Table IV summarizes several current designs of the resonance-type scanners.

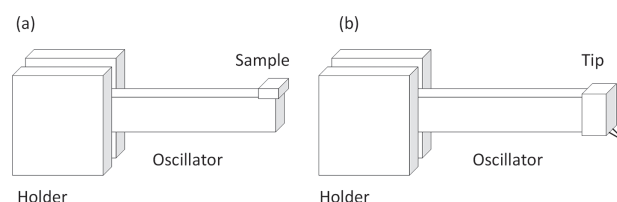


Fig. 4. The configuration of resonance-type scanners. (a) and (b) are the sample-scan mode and tip-scan mode, respectively.

Table IV. Comparison of the current designs of the resonance-type scanners.³¹

	Line scan rate (Hz)	Scan range (μm)	Motion sensing	Average tip-sample velocity (mm/s)	References
Tuning fork	~20–100 k	~0.5–5	Current	~200	[8, 77]
Brass bar	~5–10 k	1–3	\	~10	[19, 29, 30]
Quartz bar	~1 k	~37.5	\	~14–58	[78, 79]
Bimorph beam	~1–10 k	~20–40	Voltage	~120	[31, 32, 35]

The turning fork resonance-type scanner can achieve video-rate⁷⁶ and ultrafast imaging speed (1300 FPS). The images of the collagen fibers in liquid environment can be obtained.⁷⁷ However, because the system lacks electrical feedback control of the Z-scanner, cantilever deflection data are collected for imaging. Since the imaging mode is the constant-height mode, the use of softer cantilevers would be helpful to decrease the wear between the tip and the sample.⁷⁶ And samples are required to be very stable especially in liquid environment. Conventional Z-scanner can be used to provide Z height control on a frame-by-frame timescale, which might be helpful when the sample has a tilting angle. The non-linear displacement caused by the sinusoidal scan can be corrected using the post-processing method⁸⁰ or in real-time data collection system.³⁵

2.4. Z-Scanner

2.4.1. Fast Piezo Stacks Z-Scanner

The design of Z-scanner is the most complicated work in high-speed AFM. Z-scanner's operating frequency is much higher than that of XY scanner. The design methods and configurations of Z-scanner were summarized in Ando's review¹⁰ and also in Yong's review.⁵⁷ In our opinion, the most convenient method is to use a small piezo element to provide fast displacement vertically. For example, Liao et al. used a small piezo plate stack (NAC2012, Noliac) as high-speed Z-scanner. The plate has the dimensions of $3 \times 3 \times 2$ mm and its maximum free stroke is $\sim 3 \mu\text{m}$.¹³ The unload resonance frequency of the piezo plate can be larger than 486 kHz. After fixing the piezo plate on the XY scanner and attaching a sample holder to it, the measured Z-resonance frequency can achieve ~ 44.4 kHz.¹³ Miyata et al. used a multilayer piezo plate (PL033, PI Ceramics) with the same size ($3 \times 3 \times 2$ mm). Due to the fact that the configuration is tip-scan AFM, one side of the piezo plate is fixed to the main body made of stainless steel and the other side is glued with a stage for the cantilever. The normal vibration mode is ~ 110 kHz and different cantilever holding methods would affect the resonance frequency.⁸¹ The cantilever holder that has a small mass should be able to clamp the chip firmly without deteriorating Z-scanner's fast performance, and repeated exchanges of cantilever chips should not damage the Z-scanner. To meet these requirements, Fukuda et al. presented a novel design to hold cantilever chip which was indirectly mounted on Z-scanner

and did not affect the fast and precise response of the Z-scanner.⁸² Braunsma et al. used a piezo stack with the dimensions of ($5 \times 5 \times 2$ mm) and a fundamental resonance frequency of ~ 150 kHz if clamped at one end. The measured result and the FEA simulation indicate that the Z resonance frequency is ~ 35 kHz after sticking a sample stage on it and the maximum Z-displacement is $3.3 \mu\text{m}$.¹⁶ To compensate for Z-piezo's nonlinearity, creep, and hysteresis, a high-speed displacement sensor with sub-nanometer resolution was proposed based on an optical knife-edge technique.⁸³ With this sensor, the nonlinear Z-piezo displacements can be detected and corrected during high-speed force curve measurements. In combination with small cantilevers, high-speed force mapping can be reached, which is 10–100 times faster compared to conventional force mapping.⁸⁴

Though the displacement range of compact piezo component is very limited, it is enough for the observation of samples with smooth surfaces and some biological applications. In order to design a more general purpose Z-scanner, longer piezo actuators with longer strokes would be more suitable. In Ando's early designs, they used piezo stacks with dimensions of $3.5 \times 4.5 \times 5$ mm and maximum displacement of $\sim 4.6 \mu\text{m}$. Its resonance frequency is ~ 261 KHz when there is no mechanical load.⁷ However, quick displacement of the piezo stack exerts an impulsive force to its supporting base, which would cause vibrations of the surrounding structures and in turn affect the piezo stack itself.⁵³ Therefore, they proposed a counterbalance method to circumvent this problem where two piezo stacks were attached to the opposite faces of the supporting base. One piezo stack actuator was used to support the sample stage and a dummy stage that has the same mass as the sample stage was attached to the other Z-piezo actuator.⁷ In this way, the impulsive forces exerted to the supporting base were cancelled with each other. In their later designs, this method was also applied to X-axis (fast axis) of the scanner.^{56, 85, 86} Similar designs to suppress the oscillation of Z-scanner can also be found in the works of Hansma's group^{71, 74, 87} and MIT high-speed AFM.^{88, 89} This counterbalance method can also be embedded in tip-scan configurations.^{52, 82}

Combined with the commercially available AFM system, Fleming and Kenton et al. developed a high-speed vertical positioner.^{38, 39} The counterbalance method was employed with two 2-mm thick piezo stack actuators. The piezo

stacks have the alumina end caps (each 0.65 mm thick) for electrical isolation. To further increase the resonance frequency, a circular plate flexure was used to enhance the stiffness in transverse directions (X and Y) and to guide the sample mass in Z -direction. With the counterbalanced mechanical design and the circular flexure, the resonance frequency and the scan range can achieve 103 kHz and $\sim 2.3 \mu\text{m}$, respectively. Integrating Z -scanner with conventional AFM, the closed-loop bandwidth was increased from 83 Hz to 67 kHz, an improvement of over 800 times. The vertical feedback was demonstrated to provide excellent feature tracking at line scan rate of 200 Hz.^{38,39}

Other “inertia balance” methods using just one single piezo actuator as Z -scanner were summarized in Ando’s review.¹⁰ One design employs a piezoelectric actuator sandwiched between two flexures in displacement directions. As a single actuator is used, its center of mass as well as the entire mechanism barely move when the mechanical properties of the two flexures are similar to each other. Another way is that a piezo actuator is held only at the rims or corners of a plane perpendicular to the displacement direction. This allows the actuator to be displaced almost freely in both directions and the center of mass barely moves. The third way is to mount a small piezo actuator ($2 \times 2 \times 2 \text{ mm}$) inside a hole at the center of the support to ensure that it is supported on all four sides but not at each end. As such, when the piezo actuator is extended or retracted, it does so in both directions symmetrically. Therefore, there is no imbalance from a change of center mass.^{12,90} The Z -axis resonance frequency can achieve 540 kHz in this case.⁹⁰

2.4.2. Dual-Actuator Z -Scanner

Alternative method to overcome the limited Z -range is the combination of a compact piezo component with a conventional piezo scanner, such as adding an extra Z -actuator to the original AFM to form a dual-actuated Z -scanner. The advantage of this method is that it can be performed on an existing AFM system without a lot of mechanical changes. For example, in a conventional tip-scan AFM, a stack-piezo (PICMA Physik instrumente, Germany) with nominal resonance frequency $>300 \text{ kHz}$ was added below the sample.⁹¹ In similar designs, a ring multi-layer piezoelectric disk (CMAR02, Noliac, Denmark) with a diameter of 8 mm

(nominal resonance frequency $>486 \text{ kHz}$) was employed as high-speed positioner.⁹² The ring-stack actuator that serves as fast Z -scanner can be further enhanced with circular flexures. A 0.254 mm thick circular flexure was glued on top of the ring actuator and into the counter bore of the base plate. The vibration frequency (piston mode) of Z -scanner was increased to $\sim 88 \text{ kHz}$.⁹³

For conventional sample-scan AFM (Bruker Multi-Mode AFM), Kuiper et al. used a small piezoelectric plate actuator (CMAP12, Noliac, Denmark) which was glued onto the cantilever holder to form the new mounting spot for cantilever-chip and allowed vertical positioning of the cantilever-chip with a maximum range of about $0.5 \mu\text{m}$.⁹⁴ In MIT high-speed AFM system,⁹⁵ a small ($2 \times 2 \times 2 \text{ mm}$) piezo-stack, model PL022.30 from PI (Physik Instrumente) is used as high speed actuator. It is enclosed in an aluminum flexure cap in order to preload the piezo-stack and protect the high voltage electrical connections when operated in fluid. The flexure cap is composed of a top aluminum diaphragm (1 mm thick) and a lower pressure screw. The piezo-stack actuator is glued to the top diaphragm and then pre-loaded from the bottom by the pressure screw.⁹⁵

The controller used for dual-actuated scanner has a frequency filter to split the deflection error signal into two complimentary parts, which are low frequency part and high frequency part. Low frequency part was used to drive the low-speed and long-range actuator, like the tube scanner.^{37,39,94} And high frequency part was applied to the piezo stack which is a fast-speed and short-range actuator. Topographic images could be obtained by collecting the sum of displacements of the two scanners.⁹⁴ Although the controller with frequency-based approach enables the tracking of both low and high frequency movements, one major challenge is that some precision positioning trajectories are not achievable. When using frequency-based approaches, low-speed and short-range inputs were diverted to the low-speed long-range actuator, which results in lower positioning resolution. To overcome this issue, with a spatial filter, the moving range was used to determine the allocation of control effort between the two actuators.⁹⁶ This allows for low-speed, short-range inputs to be followed using high-speed, high-resolution actuator. Table V summarizes the typical scheme of fast Z -scanner used in HSAFM. Typical

Table V. Summarization of the schemes of the fast Z -scanner.

Piezo actuators type	Typical model	Geometry (mm)	Scanner structure	References
Plate actuator	NAC2012	$3 \times 3 \times 2$	Single plate	[13, 16, 37, 67, 81]
Plate actuator	NAC2013	$5 \times 5 \times 2$	Counter balance/circular flexure	[38, 39]
Plate actuator	PL022.30	$2 \times 2 \times 2$	Dual actuators	[44, 95, 97]
Piezo-stacks	AE0203D04	$3.5 \times 4.5 \times 5$	Counter balance	[7, 52, 68, 71, 74, 82, 85, 87–89, 98]
Piezo-stacks	AE0203D04	$3.5 \times 4.5 \times 5$	Leaf flexure	[99]
Ring actuator	NAC2121	$6 \times 2 \times 4$	Single plate/Dual actuators	[37, 92, 93]

models of the commercially available fast piezo stack actuators were also collected in this table.

2.5. Electronic System

2.5.1. Wideband High-Voltage Amplifier

The selected piezo stack actuators for XYZ scanner usually have the unloaded resonance frequency of larger than 100 kHz. This means the bandwidth of the high-voltage amplifier (HVA) which is used to drive the piezo stacks, should be larger than this level. However, due to piezo stacks' large electrical capacitance, the bandwidth of HVA is usually limited to a few kilohertz or less.¹⁰⁰ Fleming et al. developed a new dual amplifier, which exhibited a small-signal bandwidth of 2 MHz with a 100 nF capacitive load. The dual amplifier is comprised of a standard high-voltage amplifier and a fast low-voltage amplifier to improve performance at higher frequencies.¹⁰⁰ Miyata et al. specifically designed the HVA to drive separated-type scanners which enable to achieve the positioning accuracy of 5.7 and 0.53 pm in *XY* and *Z* axes, respectively. The excellent noise performance can guarantee the experiments on atomic-resolution imaging of mica and calcite in liquid.⁸¹ In both of the proposed designs, a high-bandwidth and high-voltage operation amplifier with fast slew rate of 1000 V/us was selected, e.g., PA98 (Cirrus Logic).

2.5.2. High-Speed Data Acquisition and Control System

With the increased scan speed, the requirements for data acquisition system (DAQ) to be capable of handling the increased amount of data in real-time arise.⁷³ Fantner et al. described the dataflow in a typical HSAFM system. For example, with the intermediate imaging speed of 256×256 pixels at 10 FPS, the sample rate of the imaging system should achieve 1.3 MHz for data acquisition system. Another key function of the DAQ system is that the A/D channels should be synchronous to the D/A channels, which guarantees that each pixel can be uniquely assigned to a position in a specific line and frame.⁷³ To ensure the acquisition efficiency, DMA (Direct memory access) function is also required. The data can then be directly written to PC main memory without any processor involvement.⁷³ The Adlink DAQ-2000 series device with maximal sampling rate of 2 M and resolution of 14 bits was chosen for high-speed imaging.^{73, 87, 101} Typical results with 150×150 pixels at 30 FPS were obtained.⁸⁷ Fleming et al. pointed out that one DAQ equipment (NI PCI-6115, high-speed simultaneous sampling data acquisition card) with an analog-to-digital conversion bandwidth of 10 MS/s and a digital-to-analog conversion bandwidth of 2.5 MS/s, was sufficient for operation with 160×160 pixels at 50 FPS (line scan rate is 8 kHz).³⁸ In our HSAFM with bimorph resonance-type scanner, this DAQ device (NI PCI-6115) was employed for simultaneous scan signals and high-speed data acquisition, typical results with 100×100 pixels were

recorded at 31.6 FPS.^{31–36} For real-time user interface of HSAFM, multi-touch function was employed rather than conventional sequential approach in Miles's group, which allows the operator to interact with multiple controls simultaneously.¹⁰²

In tapping mode HSAFM, in order to reduce the interaction force during imaging, the amplitude set-point should be set close to the amplitude of free oscillation. However, when the scan speed increases, the cantilever tip tends to be detached completely from the sample surface. This would cause the imaging to be unstable. In Ando's group, Kodera et al. proposed a dynamic proportional-integral-derivative (PID) control method (the feedback control gains are automatically adjusted depending on the value of the error signal).¹⁰³ And the active damping technique was applied in all three scan directions to reduce the quality factor *Q* of *Z* actuators' resonance, so the response speed was greatly enhanced.⁹⁸ In addition, with amplitude drift compensation in the cantilever-excitation efficiency, very stable imaging was achieved.^{56, 103}

Fleming et al. used an analog integral circuit as the wideband vertical position controller. Due to the fact that their line scan rate is limited to approximately 200 Hz, a lower-cost DAQ card (NI PCI-6221) is sufficient to be employed. This device contains a 16-channel 16-bit 250 kS/s analog-to-digital converter and two 16-bit analog outputs. The experimental results demonstrate that the imaging rate for 200×200 pixels is 1 FPS.³⁸ This method is very useful to upgrade conventional AFM without significant hardware modification. Braunsman et al. also proposed an analog PID controller that the electronics have a bandwidth exceeding 1 MHz.¹⁶

Compared with the analog feedback controller, digital controllers' flexibility is much higher and thus more complex measurement tasks can be carried out.¹⁰⁴ Besides the control target required for tip-sample interactions, digital feedback controllers can also be embedded in the advanced algorithm to damp the mechanical vibrations and compensate for non-linear or crosstalk of the scanner.⁵³ Digital signal processor (DSP) can be employed which was used for the implementation of the real-time feedback controller.^{105, 106} However, for high-speed AFM, such controllers are either computationally intensive or have a high implementation cost. Dedicated hardware such as FPGA (field-programmable gate array)¹⁰⁷ or FPAA (field-programmable analog array)⁶⁷ were suitable for high-speed feedback control.

For FPGA scheme, one example is MIT high-speed AFM.^{44, 63, 89, 97, 101} Two independent FPGA platforms are used to drive the lateral and out-of-plane actuators. The out-of-plane actuators are driven by a National Instruments (NI) PXIe-7966R FlexRIO module with an NI 5781 baseband transceiver (dual 100 MS/s, 14-bit inputs and dual 100 MS/s, 16-bit outputs). The three lateral actuators are driven by an NI PXI-7851 FPGA module. The AFM coarse approach

mechanism is also implemented on this FPGA.⁴⁴ Another example was that Liao et al. used a controller which includes a real time processor (PXIe-8101), three FPGA modules (PXIe-7962R, PXIe-7961R, PXI-7851R), and two high-speed adapter modules (NI-5781). More FPGA modules are useful to execute different functions, such as feedback control, XY scanning, and resonance amplitude detection.¹³

The sampling rate of typical rapid prototyping systems may limit the implementation of requisite controllers. Thus, the field programmable analog array (FPGA) is used to implement control methods⁶⁶ because it is a direct analog controller implementation, which allows for much higher control bandwidth. A model-based feedback controller on FPA, which enables a control bandwidth beyond 100 kHz with tight control demands for high-speed AFM imaging at reduced variations of imaging force, was implemented by Schitter and Phan.^{91,108} Also an FPA development board (AN231K04, Anadigm) was used to implement the controllers to sufficiently damp the structural resonances and reduce the hysteresis of the scanner.⁶⁶

3. CONCLUSION AND OUTLOOK

Rapid and accurate measurements with AFM are required for the observation of dynamic nanoscale phenomena occurring on sample surfaces, e.g., biological processes, polymer crystallization, and functional devices' inspections. As approaches of HSAFM continue to evolve, more scientific discoveries would be found by various researchers. This is the motivation to develop new HSAFM system. But still a considerable amount of research efforts should be focused on the improvements of each component in instrumentation like mechanical parts, optical paths, electrical components, and scan/control methods.

Future works would involve wide-range and high-resolution HSAFM imaging which could ensure to observe dynamic processes and in the meantime some fine details of the sample could also be found. This function would be very useful in explaining and understanding the physical or chemical mechanism of the observed dynamic processes. Also magnification mode can be embedded in HSAFM just like the optical microscopy or electron microscopy. Compared with conventional AFM, this function would be helpful to find the target area or structures of interest. In addition, to extend high-speed scanning methods to other SPM, such as scanning near-field optical microscope (SNOM), and to combine HSAFM with other instruments like X-ray microscope or different types of optical microscopes would become promising methods to investigate the dynamic processes with various information at micro- and nanoscale.

Acknowledgment: This work was supported by the China National Key Basic Research Program 973 (Grant No. 2013CB934004), the National Natural Science Foundation of China (Grant No.11232013, 11304006), and the

Fundamental Research Fund for the Central Universities (Grant No. YWF-13-D2-XX-14).

References and Notes

1. G. Binnig, C. F. Quate, and C. Gerber, *Phys. Rev. Lett.* 56, 930 (1986).
2. P. Eaton and P. West, *Atomic Force Microscopy*, Oxford University Press, New York (2010).
3. P. K. Hansma, G. Schitter, G. E. Fantner, and C. Prater, *Science* 314, 601 (2006).
4. N. Kodera, D. Yamamoto, R. Ishikawa, and T. Ando, *Nature* 468, 72 (2010).
5. T. Uchihashi, R. Iino, T. Ando, and H. Noji, *Science* 333, 755 (2011).
6. T. Uchihashi and T. Ando, *Methods Mol. Biol. (Clifton, NJ)* 736, 285 (2011).
7. T. Ando, N. Kodera, E. Takai, D. Maruyama, K. Saito, and A. Toda, *Proc. Natl. Acad. Sci. U. S. A.* 98, 12468 (2001).
8. A. D. L. Humphris, M. J. Miles, and J. K. Hobbs, *Appl. Phys. Lett.* 86, 034106 (2005).
9. G. Schitter and M. J. Rost, *Mater. Today* 11, 40 (2008).
10. T. Ando, T. Uchihashi, and T. Fukuma, *Prog. Mater. Sci.* 83, 337 (2008).
11. T. Ando, *Nanotechnology* 23, 062001 (2012).
12. B. P. Brown, L. Picco, M. J. Miles, and C. F. J. Faul, *Small* 9, 3201 (2013).
13. H.-S. Liao, Y.-H. Chen, R.-F. Ding, H.-F. Huang, W.-M. Wang, E.-T. Hwu, K.-Y. Huang, C.-S. Chang, and I.-S. Hwang, *Rev. Sci. Instrum.* 85, 103710 (2014).
14. A. Raman, J. Melcher, and R. Tung, *Nano Today* 3, 20 (2008).
15. D. A. Walters, J. P. Cleveland, N. H. Thomson, P. K. Hansma, M. A. Wendman, G. Gurley, and V. Short, *Rev. Sci. Instrum.* 67, 3583 (1996).
16. C. Braunsman and T. E. Schäffer, *Nanotechnology* 21, 225705 (2010).
17. J. H. Kindt, N. Phan, B. Pittenger, A. Mednick, A. Slade, L. Huang, W. Wang, N. Erina, J. E. Shaw, and S. C. Minne, *Bruker Appl. Note #134* 1–10 (2011).
18. T. Ando, T. Uchihashi, and N. Kodera, *Jpn. J. Appl. Phys.* 51, 08KA02 (2012).
19. D. Lee, H. Lee, N. S. Lee, K. B. Kim, and Y. Seo, *Curr. Appl. Phys.* 12, 989 (2012).
20. J. D. Adams, A. Nievergelt, B. W. Erickson, C. Yang, M. Dukic, and G. E. Fantner, *Rev. Sci. Instrum.* 85, 093702 (2014).
21. H. Kawakatsu, S. Kawai, D. Saya, M. Nagashio, D. Kobayashi, H. Toshiyoshi, and H. Fujita, *Rev. Sci. Instrum.* 73, 2317 (2002).
22. H. Kawakatsu, D. Saya, A. Kato, K. Fukushima, H. Toshiyoshi, and H. Fujita, *Rev. Sci. Instrum.* 73, 1188 (2002).
23. A. D. Slatery, A. J. Blanch, V. Ejov, J. S. Quinton, and C. T. Gibson, *Nanotechnology* 25, 335705 (2014).
24. T. Uchihashi, H. Watanabe, S. Fukuda, M. Shibata, and T. Ando, *Ultramicroscopy* 160, 182 (2016).
25. O. D. Payton, L. Picco, M. J. Miles, M. E. Homer, and A. R. Champneys, *Rev. Sci. Instrum.* 83, 083710 (2012).
26. D. M. Carberry, L. Picco, P. G. Dunton, and M. J. Miles, *Nanotechnology* 20, 434018 (2009).
27. O. D. Payton, L. Picco, D. Robert, A. Raman, M. E. Homer, A. R. Champneys, and M. J. Miles, *Nanotechnology* 23, 205704 (2012).
28. P. Klapetek, L. Picco, O. Payton, A. Yacoot, and M. Miles, *Meas. Sci. Technol.* 24, 25006 (2013).
29. Y. Seo, C. S. Choi, S. H. Han, and S. H. Han, *Rev. Sci. Instrum.* 79, 103703 (2008).
30. H. H. Lee, D. Lee, K. B. Kim, Y. Seo, H. Kim, and H. H. Lee, *Ultramicroscopy* 110, 826 (2010).
31. Y. Zhou, G. Shang, W. Cai, and J. Yao, *Rev. Sci. Instrum.* 81, 053708 (2010).

32. J. Zhao, W. Gong, W. Cai, and G. Shang, *Rev. Sci. Instrum.* 84, 083706 (2013).
33. J. Zhao, W. Cai, G. Shang, and J. Yao, *Appl. Phys. Express* 6, 075201 (2013).
34. H. Fan, W. Cai, J. Zhao, and G. Shang, A high-speed atomic friction force microscopic imaging system based on a novel optical beam deflection design, *2013 IEEE International Conference on Imaging Systems and Techniques (IST)*, IEEE (2013), pp. 437–440. doi:10.1109/IST.2013.6729737.
35. W. Cai, J. Zhao, W. Gong, H. Fan, and G. Shang, *Meas. Sci. Technol.* 25, 125404 (2014).
36. W. Cai, H. Fan, J. Zhao, and G. Shang, *Nanoscale Res. Lett.* 9, 665 (2014).
37. A. J. Fleming, *IEEE Trans. Control Syst. Technol.* 19, 156 (2011).
38. A. J. Fleming, B. J. Kenton, and K. K. Leang, *Ultramicroscopy* 110, 1205 (2010).
39. B. J. Kenton, A. J. Fleming, and K. K. Leang, *Rev. Sci. Instrum.* 82, 123703 (2011).
40. M. B. Viani, T. E. Schäffer, G. T. Palocz, L. I. Pietrasanta, B. L. Smith, J. B. Thompson, M. Richter, M. Rief, H. E. Gaub, K. W. Plaxco, A. N. Cleland, H. G. Hansma, and P. K. Hansma, *Rev. Sci. Instrum.* 70, 4300 (1999).
41. T. E. Schäffer, M. Viani, D. A. Walters, B. Drake, E. K. Runge, J. P. Cleveland, M. A. Wendman, and P. K. Hansma, Atomic force microscope for small cantilevers, *Photonics West '97*, edited by T. A. Michalske and M. A. Wendman, International Society for Optics and Photonics, (1997), Vol. 3009, pp. 48–52.
42. T. E. Schäffer, J. P. Cleveland, F. Ohnesorge, D. A. Walters, and P. K. Hansma, *J. Appl. Phys.* 80, 3622 (1996).
43. G. E. Fantner, R. J. Barbero, D. S. Gray, and A. M. Belcher, *Nanotechnology* 5, 280 (2010).
44. I. S. Bozchalooi, A. C. Houck, J. AlGhamdi, and K. Youcef-Toumi, *Ultramicroscopy* 160, 213 (2016).
45. T. Uchihashi, N. Kodera, and T. Ando, *Nat. Protoc.* 7, 1193 (2012).
46. T. Meier, A. Förste, A. Tavassolizadeh, K. Rott, D. Meyners, R. Gröger, G. Reiss, E. Quandt, T. Schimmel, and H. Hölscher, *Beilstein J. Nanotechnol.* 6, 451 (2015).
47. Y. Song, S. Wu, L. Xu, and X. Fu, *Sensors (Basel)* 15, 5865 (2015).
48. S. Fukuda, T. Uchihashi, R. Iino, Y. Okazaki, M. Yoshida, K. Igarashi, and T. Ando, *Rev. Sci. Instrum.* 84, 073706 (2013).
49. P. K. Hansma, B. Drake, D. Grigg, C. B. Prater, F. Yashar, G. Gurley, V. Elings, S. Feinstein, and R. Lal, *J. Appl. Phys.* 76, 796 (1994).
50. P. S. Jung and D. R. Yaniv, *Electron. Lett.* 29, 264 (1993).
51. S. K. Hung and L. C. Fu, Novel three-dimensional beam tracking system for stationary-sample type atomic force microscopy, *Proc. 21st IEEE Instrum. Meas. Technol. Conf.* (2006), Vol. 55, pp. 1648–1654.
52. Y. Suzuki, N. Sakai, A. Yoshida, Y. Uekusa, A. Yagi, Y. Imaoka, S. Ito, K. Karaki, and K. Takeyasu, *Sci. Rep.* 3, 2131 (2013).
53. T. Uchihashi, N. Kodera, and T. Ando, Noncontact Atomic Force Microscopy, edited by S. Morita and F. J. Giessibl, Springer International Publishing, Switzerland, (2015), Vol. 3, pp. 481–518.
54. S. O. R. Moheimani, *Rev. Sci. Instrum.* 79, 071101 (2008).
55. M. J. Rost, L. Crama, P. Schakel, E. van Tol, G. B. E. M. van Velzen-Williams, C. F. Overgaw, H. ter Horst, H. Dekker, B. Okhuijsen, M. Seynen, A. Vijftigschild, P. Han, A. J. Katan, K. Schoots, R. Schumm, W. van Loo, T. H. Oosterkamp, and J. W. M. Frenken, *Rev. Sci. Instrum.* 76, 053710 (2005).
56. T. Ando, T. Uchihashi, N. Kodera, D. Yamamoto, A. Miyagi, M. Taniguchi, and H. Yamashita, *Pflügers Arch. - Eur. J. Physiol.* 456, 211 (2008).
57. Y. K. Yong, S. O. R. Moheimani, B. J. Kenton, and K. K. Leang, *Rev. Sci. Instrum.* 83, 121101 (2012).
58. M. V. Vitorino, Development of a beamline high speed atomic force microscope and tuning of a mechanical oscillator via a force feedback strategy [dissertation], Lisboa, Universidade de Lisboa (2014).
59. Y. K. Yong, S. O. R. Moheimani, and I. R. Petersen, *Nanotechnology* 21, 365503 (2010).
60. A. Bazaei, Y. K. Yong, and S. O. R. Moheimani, *Rev. Sci. Instrum.* 83, 063701 (2012).
61. Y. K. Yong, A. Bazaei, S. O. R. Moheimani, and F. Allgower, Design and control of a novel non-raster scan pattern for fast scanning probe microscopy, *IEEE/ASME Int. Conf. Adv. Intell. Mechatronics, AIM* (2012), pp. 456–461, doi:10.1109/AIM.2012.6266062.
62. Y. K. Yong, A. Bazaei, and S. O. R. Moheimani, *IEEE Trans. Nanotechnol.* 13, 85 (2014).
63. I. S. Bozchalooi, K. Youcef-Toumi, D. J. Burns, and G. E. Fantner, *Rev. Sci. Instrum.* 82, 113712 (2011).
64. A. J. Fleming, *Sensors Actuators A Phys.* 190, 106 (2013).
65. S. Polit and J. Dong, *IEEE/ASME Trans. Mechatronics* 16, 724 (2011).
66. Y. K. Yong, B. Bhikkaji, S. O. R. Moheimani, *IEEE/ASME Trans. Mechatronics* 18, 1060 (2013).
67. S. P. Wadikhaye, Y. K. Yong, and S. O. R. Moheimani, *Rev. Sci. Instrum.* 85, 105104 (2014).
68. Y. K. Yong and S. O. R. Moheimani, *IEEE Trans. Nanotechnol.* 14, 338 (2015).
69. P. Klapetek, M. Valtr, L. Picco, O. D. Payton, J. Martinek, A. Yacoot, and M. Miles, *Nanotechnology* 26, 065501 (2015).
70. H. Watanabe, T. Uchihashi, T. Kobashi, M. Shibata, J. Nishiyama, R. Yasuda, and T. Ando, *Rev. Sci. Instrum.* 84, 053702 (2013).
71. J. H. Kindt, G. E. Fantner, J. A. Cutroni, and P. K. Hansma, *Ultramicroscopy* 100, 259 (2004).
72. S. P. Wadikhaye, Y. K. Yong, and S. O. R. Moheimani, *Micro Nano Lett.* 7, 309 (2012).
73. G. E. Fantner, P. Hegarty, J. H. Kindt, G. Schitter, G. A. G. Cidade, and P. K. Hansma, *Rev. Sci. Instrum.* 76, 026118 (2005).
74. G. Schitter, K. J. Åström, B. E. DeMartini, P. J. Thurner, K. L. Turner, P. K. Hansma, K. J. Astrom, B. E. DeMartini, P. J. Thurner, K. L. Turner, and P. K. Hansma, *IEEE Trans. Control Syst. Technol.* 15, 906 (2007).
75. K. K. Leang and A. J. Fleming, *Asian J. Control* 11, 144 (2009).
76. J. K. Hobbs, C. Vasilev, and A. D. L. Humphris, *Analyst* 131, 251 (2006).
77. L. Picco, L. Bozec, A. Ulcinas, D. J. Engledew, M. Antognozzi, M. Horton, and M. J. Miles, *Nanotechnology* 18, 044030 (2007).
78. B. Zhao, J. P. Howard-Knight, A. D. L. Humphris, L. Kailas, E. C. Ratcliffe, S. J. Foster, and J. K. Hobbs, *Rev. Sci. Instrum.* 80, 093707 (2009).
79. A. D. L. Humphris, B. Zhao, D. Catto, J. P. Howard-Knight, P. Kohli, and J. K. Hobbs, *Rev. Sci. Instrum.* 82, 043710 (2011).
80. L. Xu, X. Tian, X. Li, G. Shang, and J. Yao, *Meas. Sci. Technol.* 22, 114023 (2011).
81. K. Miyata, S. Usho, S. Yamada, S. Furuya, K. Yoshida, H. Asakawa, and T. Fukuma, *Rev. Sci. Instrum.* 84, 043705 (2013).
82. S. Fukuda, T. Uchihashi, and T. Ando, *Rev. Sci. Instrum.* 86, 063703 (2015).
83. C. Braunsman and V. Prucker, and T. E. Schäffer, *Appl. Phys. Lett.* 104, 103101 (2014).
84. C. Braunsman, J. Seifert, J. Rheinlaender, and T. E. Schäffer, *Rev. Sci. Instrum.* 85, 073703 (2014).
85. T. Ando, N. Kodera, T. Uchihashi, A. Miyagi, R. Nakakita, H. Yamashita, and K. Matada, *e-Journal Surf. Sci. Nanotechnol.* 3, 384 (2005).
86. T. Uchihashi, N. Kodera, and T. Ando, Atomic Force Microscopy in Nanobiology, edited by K. Takeyasu, Pan Stanford Publishing, Boca Raton (2014), pp. 143–176.
87. G. E. Fantner, G. Schitter, J. H. Kindt, T. Ivanov, K. Ivanova, R. Patel, N. Holten-Andersen, J. Adams, P. J. Thurner, I. W. Rangelow, and P. K. Hansma, *Ultramicroscopy* 106, 881 (2006).
88. D. J. Burns, G. E. Fantner, and K. Youcef-Toumi, *2012 Am. Control Conf.* 3240 (2012).

89. I. S. Bozchalooi, K. Youcef-Toumi, D. J. Burns, G. E. Fantner, and F. Q. Elizabeth, *2012 Am. Control Conf.* 3797 (2012).
90. T. Fukuma, Y. Okazaki, N. Kodera, T. Uchihashi, and T. Ando, *Appl. Phys. Lett.* 92, 243119 (2008).
91. G. Schitter, W. F. Rijkée, and N. Phan, Dual actuation for high-bandwidth nanopositioning, *Proc. IEEE Conf. Decis. Control* (2008), pp. 5176–5181. doi:10.1109/CDC.2008.4738876.
92. A. J. Fleming, High-speed vertical positioning for contact-mode atomic force microscopy, *2009 IEEE/ASME Int. Conf. Adv. Intell. Mechatronics* (2009), pp. 522–527, doi:10.1109/AIM.2009.5229959.
93. A. J. Fleming, B. J. Kenton, and K. K. Leang, *2010 Am. Control Conf.*, 4975, (2010).
94. S. Kuiper, A. J. Fleming, and G. Schitter, Dual actuation for high speed atomic force microscopy, *Proc. IFAC Mechatronics Conf.*, edited by C. George (2010), pp. 220–226.
95. I. Soltani Bozchalooi and K. Youcef-Toumi, *Ultramicroscopy* 146, 117 (2014).
96. G. M. Clayton, C. J. Dudley, and K. K. Leang, *Rev. Sci. Instrum.* 85, 045003 (2014).
97. I. S. Bozchalooi and K. Youcef-Toumi, *2014 Am. Control Conf.*, 1643 (2014), doi:10.1109/ACC.2014.6859262.
98. N. Kodera, H. Yamashita, and T. Ando, *Rev. Sci. Instrum.* 76, 053708 (2005).
99. Y. K. Yong and S. O. R. Moheimani, A compact XYZ scanner for fast atomic force microscopy in constant force contact mode, *2010 IEEE/ASME International Conference on Advanced Intelligent Mechatronics*, IEEE (2010), pp. 225–230, doi:10.1109/AIM.2010.5695880.
100. A. J. Fleming, *Rev. Sci. Instrum.* 80, 104701 (2009).
101. D. J. Burns. A System Dynamics Approach to User Independence in High Speed Atomic Force Microscopy [dissertation], Massachusetts Institute of Technology, Boston (MA) (2010).
102. D. M. Carberry, L. Picco, P. G. Dunton, and M. J. Miles, *Nanotechnology* 20, 434018 (2009).
103. N. Kodera, M. Sakashita, and T. Ando, *Rev. Sci. Instrum.* 77, 083704 (2006).
104. D. R. Baselt, S. M. Clark, M. G. Youngquist, C. F. Spence, and J. D. Baldeschwieler, *Rev. Sci. Instrum.* 64, 1874 (1993).
105. G. Schitter and A. Stemmer, *Microelectron. Eng.* 67–68, 938 (2003).
106. G. Schitter, F. Allgöwer, and A. Stemmer, *Nanotechnology* 15, 108 (2004).
107. F. Esch, C. Dri, A. Spessot, C. Africh, G. Cautero, D. Giuressi, R. Sergo, R. Tommasini, and G. Comelli, *Rev. Sci. Instrum.* 82, 053702 (2011).
108. G. Schitter and N. Phan, *2008 Am. Control Conf.* 2690 (2008), doi: 10.1109/ACC.2008.4586899.